# *Spatial Control of Gene Expression by Nanocarriers Using Heparin Masking and Ultrasound-Targeted Microbubble Destruction*



**Citation:** Chertok, Beata et al. Spatial Control of Gene Expression by Nanocarriers Using Heparin Masking and Ultrasound-Targeted Microbubble Destruction 10, 8 (July 2016): 7267-7278 © 2016 American Chemical Society

**As Published:** http://dx.doi.org/10.1021/acsnano.6b01199

**Publisher:** American Chemical Society (ACS)

**Persistent URL:** https://hdl.handle.net/1721.1/122008

**Version:** Author's final manuscript: final author's manuscript post peer review, without publisher's formatting or copy editing

HHS Public Access

Author manuscript

*ACS Nano*. Author manuscript; available in PMC 2017 August 23.

Published in final edited form as:

*ACS Nano*. 2016 August 23; 10(8): 7267–7278. doi:10.1021/acsnano.6b01199.

# Spatial Control of Gene Expression by Nanocarriers Using Heparin Masking and Ultrasound-Targeted Microbubble Destruction

**Beata Chertok**[†,‡], **Robert Langer**[§,‖,⊥,▽], and **Daniel G. Anderson**[§,‖,⊥,▽]

[†]Department of Pharmaceutical Sciences, College of Pharmacy, University of Michigan, Ann Arbor, Michigan 48109, United States

[‡]Department of Biomedical Engineering, College of Engineering, University of Michigan, Ann Arbor, Michigan 48109, United States

[§]Department of Chemical Engineering, MIT, Cambridge, Massachusetts 02139, United States

[‖]David H. Koch Institute for Integrative Cancer Research, MIT, Cambridge, Massachusetts 02139, United States

[⊥]Institute for Medical Engineering & Science, MIT, Cambridge, Massachusetts 02139, United States

[▽]Harvard-MIT Division of Health Sciences & Technology, Cambridge, Massachusetts 02139, United States

## Abstract

We developed a method to spatially control gene expression following nonviral delivery of DNA. This method includes surface-modifying DNA nanocarriers with heparin to inhibit passive gene transfer in both the target and the off-target tissues and using ultrasound-targeted microbubble destruction (UTMD) to selectively activate heparin-inhibited gene transfer at the target site. We observed that the engraftment of heparin onto the surface of cationic liposomes reduced off-target gene expression in the liver, a major site of nanoplex accumulation, by more than 700-fold compared to the nonheparinized PEGylated liposomes. We further observed that tumor-directed UTMD increased gene transfer with heparin-modified nanoplexes by more than 10-fold. This method augmented tumor-to-liver selectivity of gene expression by 4000-fold compared to controls. We conclude that heparinization of DNA nanocarriers in conjunction with localized activation of gene transfer by UTMD may enable greater spatial control over genetic therapy.

## Graphical abstract

Correspondence to: Daniel G. Anderson.

Supporting Information: The Supporting Information is available free of charge on the ACS Publications website at DOI: 10.1021/acsnano.6b01199.

Optimization of the postinsertion procedure, microbubble characterization, spectral characterization of Cy5.5-labeled liposomes. (PDF)

**Notes**: The authors declare no competing financial interest.

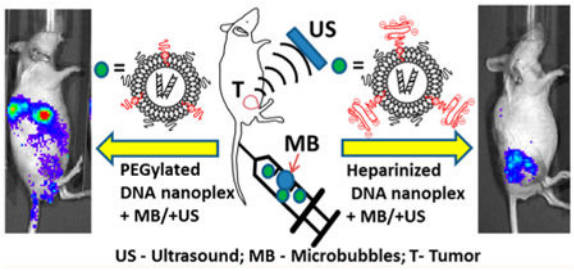


**Keywords**

gene delivery; spatial control; tumor targeting; gene nanocarriers; heparin surface masking; microbubbles; ultrasound

Targeted systemic gene delivery has the potential to treat a range of intractable diseases including cancer.[1,2] Localized transfer of genetic materials to target cells has been explored for altering cell signaling or used as a pharmacological approach to kill diseased cells. A next step in developing gene therapy is to spatially target specific cells *in vivo* with minimal alteration of gene expression to healthy cells.[3] A wide variety of lipid- and polymer-based materials have been investigated as vehicles to condense plasmid DNA into nanoplexes that facilitate cellular gene transfer.[4–6] However, the systemic delivery of these vectors to specific tissues *in vivo*, with the exception of the liver and the lungs, has remained challenging.[3]

Following intravascular administration, nanoplexes are primarily cleared from circulation by "first-pass" organs such as the lungs and the liver.[7] For targets such as peripheral tumors that are situated outside the liver and the lungs, alterations of gene expression by uptake of engineered nanoplexes in first-pass organs is an undesirable side effect that poses significant toxicity concerns.[3] Many promising protein therapeutics (*e.g.*, IL12 cytokine) considered for cancer gene therapy failed in clinical trials because of hepatic and pulmonary toxicity.[3,8,9] Thus, blockage of unwanted gene expression in these organs has the potential to reduce toxicity and improve therapeutic benefit.

Approaches for improving target selectivity of peripheral gene expression include development of gene carriers that are responsive to external localized physical triggers.[10] One methodology is based on ultrasound and microbubbles.[11] Microbubbles are gas-filled microparticles that collapse under target-directed ultrasound. The associated mechanical effects can increase local permeability of tissue and cell membranes to DNA nanoplexes and augment gene transfer at target sites.[11–13] However, following systemic administration nanoplexes or nanoplex-carrying microbubbles are also subjected to passive distribution and clearance with a large fraction of the dose inevitably localizing in the liver. Despite localized activation, transfection-competent nanoplexes still pose a risk of off-target gene expression and toxicity.[3]

Although off-target gene expression has been recognized as an important barrier for gene carrier translation, only a handful of strategies have been developed to address this

challenge. PEGylation is the method of choice for reducing nonspecific gene transfer. However, the robustness of PEG protection varies markedly with nanoplex composition, PEGylation density, methods of PEG insertion and the administered dose.[14–17] Despite a PEGylated surface, gene carriers can preserve *in vivo* transfection competency and facilitate gene transfer off-target.[16,18] Therefore, alternative strategies are needed to improve target selectivity of *in vivo* gene expression.

Herein, we develop a spatially controlled method to target gene transfer following systemic administration. We reasoned that spatial definition of *in vivo* gene expression could be improved by first inhibiting passive gene transfer to reduce the background of nonselective expression and subsequently activating gene expression at the target. This approach was inspired by two phenomena. First, it is known that cationic liposomes and polyplexes mediate cellular transfection *via* electrostatic interactions with heparin-bearing anionic proteoglycans on a cell's surface.[19] Heparin and other anionic polysaccharides can block transfection by disrupting these interactions.[19] We hypothesized that engrafting heparin onto the surface of cationic liposomes could inhibit systemic gene transfer in both the target and the off-target organs. Second, it is also known that, in contrast to passive transfection, physical methods of gene transfer such as ultrasound-targeted microbubble destruction (UTMD) and electroporation act *via* direct transient permeabilization of cell membranes, which is independent of molecular interactions at a cell's surface. Gene transfer *via* active cell membrane permeabilization is insensitive to the presence of anionic polysaccharides.[19] Thus, we further hypothesized that UTMD could override heparin-based blockage of gene transfer and could selectively promote gene delivery at the target site.

Our results support feasibility of this approach. Surface masking of cationic liposomes with heparin reduced passive expression of the luciferase gene in the liver by more than 700 fold. In addition, selective application of UTMD at the target tumor site could locally override heparin-induced inhibition of liposomal gene transfer. Overall, heparinization of liposomes in conjunction with UTMD increased tumor-to-liver selectivity of gene transfer by 4000-fold compared to control nonheparinized liposomes with or without UTMD.

## Results/Discussion

### Formation and Characterization of Heparin-Functionalized DNA-Encapsulating Liposomes

To prepare heparinengrafted DNA liposomes (DNAlipHep), we synthesized lipid–PEG–heparin conjugate (HepPL, Figure 1A) and incorporated this conjugate into DNA liposomes (DNAlip, Figure 1B). Previous attempts to modify the surface of cationic lipoplexes with heparin have encountered challenges.[20] Free heparin disrupts lipoplexes because it electrostatically competes with anionic plasmid DNA (pDNA) for binding to cationic lipoplex components.[20] To circumvent charge-based competition and liposome disruption by heparin, we synthesized an amphiphilic lipid–PEG–heparin conjugate (Figure 1A). Lipid–PEG conjugates have been previously demonstrated to self-insert into a liposome's shell *via* hydrophobic interactions.[14,21] We reasoned that because the liposomal insertion of the lipid-PEG-heparin conjugate would rely on hydrophobic rather than electrostatic interactions, the conjugate, in contrast to free heparin, would allow for display of heparin on the surface without liposomal disruption.

The lipid–PEG–heparin conjugate (HepPL) was synthesized *via* a three-step procedure (Figure 2A) including: (1) chemical fragmentation of heparin to produce low molecular weight heparin (LMWH, 5–10 kDa) fragments with a terminal aldehyde-containing 2,5-anhydromannose, (2) end-chain thiolation of heparin fragments, and (3) thiol-Michael addition of thiolated heparin fragments to maleimide (MAL)-functionalized lipid–PEG (DSPE-PEG(2 kDa)-MAL). HepPL conjugate formation was evaluated by agarose gel electrophoresis (Figure 2B). Migration distance of the purified HepPL (lane d, 4.37 ± 0.15 cm) was significantly shorter ($p < 0.001$) than that of the fragmented LMWH 5–10 kDa (lane a, 6.25 ± 0.21 cm), and significantly longer ($p < 0.001$) than that of DSPE-PEG(2 kDa)-MAL (lanes b, 1.87 ± 0.17 cm), confirming successful conjugation. Spectrophotometric quantification demonstrated a 1:1 molar ratio of PEG and Heparin moieties in the purified HepPL, further corroborating formation of a linear end-to-end conjugate.

To incorporate the conjugate into the liposomal shell, we modified a previously reported postinsertion procedure.[21] We carried out postinsertion in the presence of ethanol to mildly destabilize lipid bilayers and allow transfer of HepPL conjugate into preformed liposomes from a micelle phase (Supporting Information). We optimized the method parameters (*i.e.*, ethanol concentration and liposomes/HepPL incubation ratios) to maximize HepPL insertion while minimizing liposomal disruption (Figure 3). Under optimized postinsertion conditions (37 °C, 20% ethanol, DNA/insert ratio = 0.7), we were able to achieve conjugate insertion (1.4 nmol heparin/$\mu$g liposomal DNA) as well as high recovery of liposomal DNA (~80%). DNAlipHep liposomes formulated under these conditions were used in all subsequent studies.

To confirm heparin surface engraftment in the DNAlipHep liposomes, we performed analyses using dynamic and electrophoretic light scattering, cryoTEM and anion exchange chromatography. Liposomes (DNAlipPEG) engrafted with lipid–PEG conjugates (DSPE-methoxy PEG (2 kDa)) were used as a control (Figure 4A.a). DNAlipHep (Figure 4A.b) displayed a statistically significant positive shift in hydrodynamic diameter and a statistically significant negative shift in ζ-potential compared to the DNAlipPEG controls (Figure 4B and C; diameter, 140 ± 8 nm *vs* 109 ± 11 nm; $p < 0.001$; ζ-potential, −31 ± 4 mV *vs* −2 ± 3 mV; $p < 0.001$). The higher hydrodynamic diameter and the lower ζ-potential for DNAlipHep indicated liposomal insertion of HepPL and surface display of heparin, respectively.

CryoTEM micrographs revealed that both HepPL- and lipid–PEG-modified liposomal formulations comprised predominantly (>90%) mixtures of unilamellar and bilamellar vesicles (Figure 4D). Similar morphologies of DNA liposomes were reported in previous studies.[23,24] On CryoTEM, DNAlipHep liposomes had a significantly higher diameter than the DNAlipPEG liposomes (unilamellar, 110 ± 16 nm *vs* 95 ± 15 nm, $p < 0.001$; bilamellar, 112 ± 19 nm *vs* 93 ± 13 nm, $p < 0.001$) (Figure 4E), consistent with the dynamic light scattering results. Notably, the bilamellar subpopulations of the DNAlipPEG and the DNAlipHep liposomes displayed interesting morphological differences. Although there was no significant size difference between the inner compartments of DNAlipPEG and DNAlipHep bilamellar liposomes (67 ± 11 nm *vs* 70 ± 13 nm, $p = 0.07$), the outer shell diameter was significantly larger for the DNAlipHep than for the DNAlipPEG liposomes (41

± 17 nm *vs* 26 ± 7 nm, $p < 0.001$). This difference in morphology indicated the HepPL incorporation into the outer liposomal shell.

To further validate surface accessibility of the engrafted heparin chains, we also compared DNAlipPEG and DNAlipHep using anion exchange chromatography (Figure 4F). DNAlipPEG liposomes could be eluted from the quaternary-ammonium column matrix with the flow through. In contrast, DNAlipHep were retained by the cationic matrix and required a 2 M concentration of sodium chloride for elution. This finding was consistent with a negative zeta-potential shift for the DNAlipHep and provided additional evidence for display of anionic heparin on the liposomal surface. Taken together, the results from DLS, electrophoretic light scattering, cryoTEM, and anion exchange chromatography firmly corroborated surface engraftment of heparin in DNAlipHep formulations.

We next tested the effect of heparin surface modification on stability of liposomal DNA in the presence of serum. DNAlipPEG (control) and DNAlipHep (test) formulations were incubated with serum (fetal bovine serum, FBS, 50%) and phosphate-buffered saline (PBS) for 30 min. Serum stability was defined as percent of PBS-stable DNA liposomes that remained intact following incubation with serum. Treatment with the liposome-disrupting detergent Triton X-100 revealed that both DNAlipPEG and DNAlipHep formulations maintained serum stability for at least 30 min, with only a fraction of free DNA detectable prior to detergent treatment (Figure 5A). The serum stability of the test DNAlipHep formulation did not differ significantly from that of the DNAlipPEG control (Figure 5B, 95 ± 8% *vs* 86 ± 7%, $p = 0.26$), revealing that heparin surface engraftment had no destabilizing effect on the liposomal formulation. Because PEGylated DNA liposomes have been previously demonstrated to maintain circulation stability,[24] these results suggested that DNAlipHep could also be stable in circulation and suitable for systemic administration.

## Engraftment of Heparin onto the Surface of DNA-Encapsulating Liposomes Inhibits Systemic Gene Transfer

To test whether heparin engraftment could inhibit *in vivo* liposomal gene transfer, we assessed the profiles of biodistribution and gene expression of the heparinized and the nonheparinized liposomes in tumor bearing mice. Liposomal formulations were administered by intravenous injection. At 24 h postinjection, the control nonheparinized liposomes DNAlip-PEG were found to accumulate predominantly in the liver (Figure 6, A1–2). Notwithstanding the display of PEG on liposomal surface, liver accumulation was associated with liver gene expression (4300 ± 400 R.L.U./mg tissue). Although PEG is widely utilized for preventing nonspecific gene transfer, it was previously reported that, despite PEGylated surface, cationic gene carriers remain susceptible to opsonization with complement components and subsequent cell uptake[17,25] and can preserve transfection competency.[14,16–18,26] Our results showing liver gene expression with DNAlipPEG are consistent with these reports.

In contrast to nonheparinized DNAlipPEG, heparinized DNAlipHep liposomes showed negligible gene expression in all organs including the liver. Specifically, in the liver, the major site of gene expression facilitated by nonheparinized DNAlip-PEG, heparinized DNAlipHep resulted in a 700-fold reduction of gene expression compared to the

DNAlipPEG controls (Figure 6, B1–2; 6 ± 4 R.L.U./mg tissue *vs* 4300 ± 400 R.L.U./mg tissue, $p < 0.001$). This reduction in gene transfer could not be attributed to heparin-related biodistribution effects, as the extents of liver accumulation for the DNAlipHep and the DNAlipPEG liposomes did not differ significantly (DNAlipHep *vs* DNAlipPEG: 87 ± 4% dose/organ and 80 ± 9% dose/organ, respectively, $p = 0.15$). Notably, the luminescence signal in the liver of DNAlipPEG-administered animals was found to significantly increase from 24 to 48 h postinjection, suggesting continued increase in liver gene expression over time (Figure 6, C1–2; $3 \times 10^6 \pm 1 \times 10^6$ p/sec *vs* $7 \times 10^6 \pm 2 \times 10^6$ p/sec, $p = 0.002$). In contrast, liver gene expression in DNAlipHep-injected animals remained negligible 48 h postinjection, and no significant difference was observed for the 24 h and the 48 h time points ($2 \times 10^5 \pm 9 \times 10^4$ p/sec *vs* $3 \times 10^5 \pm 7 \times 10^4$ p/sec, $p = 0.99$). These results indicate that modification of liposomal surface with heparin could indeed inhibit the *in vivo* nonspecific gene transfer.

## UTMD Can Override Heparin-Based Blockage of Gene Transfer and Selectively Activate Gene Expression at the Tumor Site

We next examined whether UTMD could override heparin-based blockage of gene transfer and activate gene transfer selectively at the tumor site.

We began by looking at the effect of UTMD *in vitro* (Figure 7). No transfection was observed following incubation of HeLa cells with the DNAlipHep liposomes with or without ultrasound or following incubation of HeLa cells with the combination of the DNAlipHep liposomes and microbubbles. In contrast, exposure of cells to the DNAlipHep liposomes and microbubbles under ultrasound (our UTMD protocol) significantly enhanced the extent of gene expression ($p < 0.001$, Figure 7). In addition, under UTMD stimulation, transfection efficiency and cell viability for the heparinized DNAlipHep liposomes did not differ significantly from the transfection efficiency and cell viability for the nonheparinized DNAlipPEG controls. (Transfection efficiency: 15200 ± 900 au *vs* 14000 ± 2000 au, $p = 0.53$; and cell viability: 77 ± 6% *vs* 74 ± 8%, $p = 0.7$). These results suggest that application of UTMD could activate gene transfer with the heparinized DNAlipHEP liposomes *in vitro* and that the activation of gene transfer *via* UTMD was as efficient for the heparinized DNAlipHep as it was for the nonheparinized DNAlipPEG liposomes.

We then explored whether similar reactivation of gene transfer by the UTMD could be carried out in tumors *in vivo* (Figure 8A). Control groups of mice that received the DNAlipHep liposomes only (control 1), the combination of the DNAlipHep liposomes and microbubbles without ultrasound (control 2), or the DNAlipHep liposomes under tumor-directed ultrasound but without microbubbles (control 3) showed essentially no gene expression in the tumor (Figure 8B and C). In contrast, mice administered with the combination of the DNAlipHep liposomes and microbubbles under tumor-directed ultrasound (the UTMD protocol) displayed more than 10-fold enhancement of gene expression in the tumor compared to controls ($p < 0.001$). This result corroborated that UTMD could override heparin-based inhibition of gene transfer *in vivo*.

Although enhancement in tumor gene expression by UTMD was also observed in mice administered with the nonheparinized DNAlipPEG liposomes (Figures 8D and E, $p =$

0.042), UTMD did not enhance tumor-to-liver selectivity of gene expression in these animals (Figure 9, $p = 0.48$). Background nonselective liver gene expression masked the small local enhancement in gene expression at the target site. In contrast, for the cohort of mice receiving DNAlipHep, the tumor-to-liver selectivity of gene expression was significantly improved by the UTMD (Figure 9, $p < 0.001$), owing to the significant reduction of the background nonspecific gene expression in the liver by DNAlipHep. Because the UTMD was selectively directed to the tumor, the DNAlipHep-induced inhibition of liver gene expression was not significantly affected by the UTMD (Figure 8B and C, $p = 0.81$). Overall, the animals treated with the combination of heparinized DNAlipHep and UTMD exhibited a 4000-fold enhancement in tumor-to-liver selectivity of gene expression compared to mice treated with the combination of nonheparinized DNAlipPEG and UTMD (Figure 9, $6 \pm 2$ *vs* $0.0012 \pm 0.0008$, $p < 0.001$). This result suggests that elimination of the “background” nonspecific gene expression by heparinization of liposomal surface augments the ability to spatially control gene transfer with the UTMD.

## Conclusions

Taken together, we demonstrate the ability of our approach to improve spatial control of gene delivery following systemic administration. Engraftment of heparin on the surface of DNA liposomes resulted in efficient inhibition of hepatic off-target gene transfer, possibly due to disruption of the electrostatic interactions between cationic nanocarriers and anionic proteoglycans on a cell's surface. Furthermore, tumor-directed UTMD overrode the heparin-induced transfection blockage and activated localized gene transfer at the tumor site, likely through direct permeabilization of cell membranes in the target tissue. This approach afforded a marked improvement in target selectivity of gene expression compared to traditional approaches. Thus, heparinization of DNA nanocarriers in conjunction with localized activation of gene transfer by UTMD may provide a strategy to spatially control gene expression following nonviral delivery of DNA.

## Methods/Experimental

### 1. Materials

Lipids including 1,2-distearoyl-*sn*-glycero-3-phosphocholine (DSPC), 1,2-distearoyl-*sn*-glycero-3-phosphoethanolamine-*N*-[methoxy(polyethylene glycol)-2000] (DSPE-mPEG(2 kDa)), 1,2-distearoyl-*sn*-glycero-3-phosphoethanol-amine-*N*-[maleimide(polyethylene glycol)-2000] (ammonium salt) (DSPE-PEG(2 kDa)-MAL) and 1,2-dioleoyl-3-trimethy-lammonium-propane (DOTAP) were obtained from Avanti Polar Lipids and used without further purification. Heterobifunctional cross-linker 3-(2-pyridyldithio)propionyl hydrazide) (PDPH) was obtained from Pierce. Heparin, sodium nitrite, 3,5-dinitrosalicylic acid, tris(bipyridine)ruthenium(II) chloride), 5,5′-dithiobis(2-nitrobenzoic acid) (Ellman's reagent), tris(2-carboxyethyl)phosphine hydrochloride (TCEP-HCl), and Triton X-100 were obtained from Sigma-Aldrich and used without further purification. Plasmid DNA encoding for reporter proteins firefly luciferase (gWiz-Luc) and GFP (gWiz-GFP) were obtained from Aldevron.

### 2. Synthesis of DSPE-PEG-LMWH Conjugate (HepPL)

HepPL conjugate was synthesized *via* a 3-step process. First, low molecular weight (5–10 kDa) heparin fragments with aldehyde-containing terminal 2,5-anhydromannose residues (LMWH-Ald) were produced by our previously reported protocol.[27]

In the second step, LMWH-Ald was modified to generate a terminal free sulfhydryl (–SH) group. A solution containing LMWH-Ald (1.4 mM of aldehyde equivalent in 100 mM phosphate buffer, pH 7.4) and 3-[2-pyridyldithio]propionyl hydrazide (PDPH, 10-fold molar excess in dimethyl sulfoxide (DMSO)) was stirred at room temperature overnight. Excess PDPH was removed by anion-exchange chromatography (HiTrap Q HP column, GE Healthcare), followed by desalting and concentration of the LMWH-PDP product using ultra-filtration. LMWH-PDP was then reduced with the tris(2-carboxyethyl) phosphine hydrochloride (TCEP-HCL, 50 mM) and purified as described above. The sulfhydryl content of the activated LMWH-SH was quantified by Ellman assay, using a well-established procedure.[28] A typical reaction yielded about 95% conversion of the terminal aldehyde group to sulfhydryl.

In the third step, the conjugate was formed by the thiol-Michael addition reaction. LMWH-SH (1.5 mM SH-equivalent, prepared in 100 mM phosphate buffer, pH 7.4) was incubated with DSPE-PEG(2 kDa)-MAL at a 1.5:1 molar ratio, at room temperature overnight. The resulting conjugate DSPE-PEG(2 kDa)-LMWH (HepPL) was purified by ultrafiltration and analyzed for content of LMWH and PEG with Azur A and barium iodine spectrophotometric assays, respectively.[27,29,30] Conjugate formation was further confirmed with agarose gel electrophoresis (1% agarose, 75 V for 1 h). Gels were visualized with Rubipy staining (1 mg/mL aqueous solution of Tris-(bipyridine)ruthenium(II) chloride), imaged with Gel Doc XR imager (Bio-Rad) and quantified by densitometry.

### 3. Preparation of Heparin-Functionalized DNA Liposomes

Liposomes encapsulating plasmid DNA were formed using a previously reported procedure.[23] Liposomes were prepared with a lipid composition of cholesterol:DSPC:DOTAP:DSPE-mPEG(2 kDa) at a mol % ratio of 55:20:15:10 and a lipid/DNA ratio of 11 $\mu$mol total lipid/mg DNA. DNA liposomes were purified from the residual free pDNA by an anion exchange chromatography (HiTrap Q HP cartridges, GE Healthcare).

To functionalize the surface of DNA liposomes with heparin, HepPL conjugate was incorporated into preformed liposomes *via* a modified postinsertion procedure. DNA liposomes were coincubated with the HepPL conjugate at 37 °C for 15 min in ethanol-containing phosphate buffered saline (PBS). Ethanol-induced liposomal destabilization was then quenched by incubation at 4 °C for 15 min. Derivatized liposomes were purified from EtOH and residual free conjugate using a tangential flow cartridge with a 500 kDa cutoff. Samples with identical composition but incubated at 4 °C for 30 min were used as controls. To optimize the postinsertion procedure, liposome-to-conjugate ratios were varied in the range of 0.1–0.7 $\mu$gDNA/nmol HepPL. In addition, the concentration of ethanol in the incubation mixtures was varied in the range of 0–30% (v/v).

Liposomal samples were analyzed for conjugate insertion and loss of encapsulated DNA. For conjugate insertion analysis, incubation mixtures (test and control) were subjected to gel electrophoresis (1% agarose, 75 V for 1 h). Gels were visualized with Rubipy staining (1 mg/mL aqueous solution of tris-(bipyridine)ruthenium(II) chloride), imaged with Gel Doc XR imager (Bio-Rad) and quantified by densitometry. Band density of the free conjugate (at migration distance of 4.4 ± 0.2 cm) was quantified for test and control samples. Liposomal insertion in test samples was calculated as % reduction in band density of the free conjugate as compared to the corresponding controls.

For analysis of the DNA loss, samples with and without 0.1% Triton X-100 were subjected to gel electrophoresis (E-gel precast agarose gels, 0.8%, 15 min). Gels were visualized with ethidium bromide, imaged with Gel Doc XR imager (Bio-Rad) and quantified by densitometry. Amount of encapsulated DNA in each sample was calculated as a difference between the total DNA released after liposomal disruption with Triton and the free nonencapsulated DNA detected without Triton. Loss of encapsulated DNA due to conjugate insertion was calculated as % reduction in encapsulated DNA in the test sample as compared to the corresponding control.

## 4. Characterization of Heparin-Functionalized DNA Liposomes

Size distribution and zeta potential of the liposomes were analyzed by dynamic and phase analysis light scattering, respectively, using ZetaPALS (Brookhaven). Liposomes were dispersed in phosphate-buffered saline (PBS), pH7.4.

Structural characterization was conducted with cryoTEM (Jeol 2100 FEG TEM, equipped with the Single Tilt Liquid Nitrogen Cryo-Transfer Holder, Gatan). For cryoTEM, samples of aqueous liposomal suspension were spotted onto a holey carbon-film coated grid (Quantifoil R5/20) and immersion-frozen with the semiautomatic cryo-plunger (CryoPlunge3, Gatan). Measurements of liposomal substructures were carried out using ImageJ.

Surface-functionalization of the liposomes was evaluated using ion exchange chromatography. DNA liposomes were formulated to contain fluorescently labeled lipid–PEG: DSPE-PEG(2 kDa)-Cy5 (0.1 mol % of lipid composition). HepPL (test) or DSPE-PEG(2 kDa) (control) were incorporated into preformed liposomes by a postinsertion procedure as described in Section 3. Test and control liposomes were loaded onto an anion exchange column (HiTrap Q HP cartridges, GE Healthcare) and eluted with a sodium chloride gradient (0–2 M). Collected fractions were analyzed for fluorescence intensity (excitation/emission at 640 nm/670 nm) using a microplate reader (Infinite 200 Pro, Tecan).

For serum stability analysis, liposomes engrafted with HepPL or DSPE-PEG(2 kDa) were incubated with fetal bovine serum (FBS, 50%) at 37 °C for 30 min. Samples incubated with PBS were used as controls. Analysis of encapsulated DNA was conducted as described in Section 3. Serum stability was calculated as percent encapsulated DNA obtained in the presence of FBS as compared to controls (incubated with PBS).

### 5. Cell Culture Experiments

For *in vitro* evaluation of liposome performance, the liposomes were formulated to contain GFP (green fluorescent protein)-encoding plasmid DNA (gWiz-GFP, Aldevron). Microbubbles (MB), comprising an octafluoropropane ($C_3F_8$, Synquest lab, FL) gas core and a DSPC/DSPE-PEG(2 kDa) shell (82:18 molar ratio), were prepared by a high-shear emulsification method.[31] Transfection experiments with and without microbubbles and acoustic stimulation were conducted in HeLa cells. HeLa cells were seeded (DMEM, 10% FBS) in acoustically transparent sealed chambers (Opticell) and allowed to grow to 70% confluence. On the day of the experiment, media was replaced with Opti-mem. Liposomal DNA (10 $\mu$g) with or without microbubbles (microbubble count: $5 \times 10^7$) was injected into the chamber and distributed evenly throughout the chamber volume. The chamber was submerged in a tank, filled with degassed water, and mounted at the focal plane of a 1 MHz piezoelectric ultrasound transducer. The transducer was driven by 1 MHz sinusoidal tone-bursts generated by an arbitrary waveform generator (Tektronix) and amplified with a 50 dB RF amplifier (E&I). Ultrasonic insonation was applied for 20 s with the following acoustic parameters: pulse duration: 33 $\mu$s, pulse repetition frequency: 3 kHz, peak negative pressure: 250 kPa. Then, 48 h post-transfection, the cells were imaged by fluorescence microscopy (excitation/emission at 470 nm (bandwidth of 22 nm)/510 nm (bandwidth of 42 nm)) and thereafter harvested and analyzed for fluorescence intensity and cell viability with fluorescence spectroscopy (excitation/emission at 485 nm/525 nm) and Trypan blue assay, respectively.

### 6. *In Vivo* Studies

All animal procedures were approved by the MIT Committee on Animal Care (CAC).

**6a. Establishment of Subcutaneous Tumors in Mice—**Murine LL/2 Lewis lung carcinoma cells (ATCC: CRL-1642) were grown as monolayers in DMEM media supplemented with 10% fetal bovine serum. For implantation, the cells were harvested by trypsinization (0.25% trypsin-EDTA, Gibco) and resuspended in sterile PBS at $2 \times 10^7$ cell/mL. Tumors were established in the rear flank of 6- to 8-week-old SCID mice (SHO, Charles River) by subcutaneous injection of cell suspension (50 $\mu$L, $1 \times 10^6$ cells). Tumors were allowed to grow for 7–14 days to a volume of 300–500 $\mu$L.

**6b. In Vivo Biodistribution and Gene Transfer—**Liposomes were formulated with the gWiz-Luc plasmid (Aldevron) encoding for reporter protein luciferase. For biodistribution analysis, the liposomes were labeled with the near-infrared dye Cy5.5 through incorporation of DSPE-PEG(2 kDa)-Cy5.5 (0.1% of lipid composition). Mice were administered liposomal suspensions (65 $\mu$g DNA) or combinations of liposomes (65 $\mu$g DNA) and microbubbles (microbubble count: $1 \times 10^9$). Suspensions were administered intravenously, *via* the lateral tail vein catheterized with a 26-gauge angiocatheter (Angiocath, Becton Dickinson, UT). For ultrasound stimulation experiments, the animals were exposed to tumor-directed acoustic insonation. The acoustic setup and insonation parameters are described under Cell Culture Experiments. Ultrasound was applied for a total of 5 min using destruction–replenishment cycles (ultrasound on for 20 s/ultrasound off for 10 s) to allow

intermittent microbubble destruction and replenishment of residual circulating microbubbles into the tumor vasculature.[32]

Biodistribution and gene expression were assessed qualitatively with the whole-body fluorescence/bioluminescence imaging and quantitatively *via* an *ex vivo* organ analysis. Fluorescence (excitation/emission at 640 nm/720 nm, epiillumination mode, exposure time = 0.5 s) and bioluminescence imaging (excitation/emission at block/open, exposure time = 300 s) was conducted using IVIS Spectrum imaging system (Xenogen). For bioluminescence imaging, mice were injected intraperitoneally with the D-luciferin substrate at 150 mg/kg. Animal organs were harvested, flash-frozen in liquid nitrogen, and stored at −80 °C until analysis.

### 7. *Ex Vivo* Analysis

For quantitative analysis of liposomebiodistribution and luciferase activity, whole mouse organs werecryogenically ground with the Geno/Grinder (Spex). Subsequently, samples of homogeneous frozen organ powder were weighed and extracted with the Glo lysis buffer (Promega), as described.[33]

Supernatants were analyzed for fluorescence intensity and luciferase activity using fluorescence spectroscopy (excitation/emission at 640 nm/710 nm) and the Bright-Glo luciferase assay system (Promega), respectively. Fluorescence/luminescence values were normalized by tissue weight and background-corrected by subtracting the fluorescence/luminescence of the corresponding tissues from nontreated control animals. Extraction procedure for quantitative biodistribution and gene expression analyses was validated through identical analyses of control tissues spiked with fluorescently labeled liposomes and a recombinant luciferase protein (QuantiLum, Promega), respectively.

### 8. Statistical Analysis

Data are expressed as mean ± S.D., unless otherwise specified. Comparisons between the two groups were made using the unpaired *t* test. Means of multiple groups were compared with the 1-way ANOVA, followed by post hoc Tukey's pairwise comparisons. Homoscedasticity was analyzed with the Levene's test. All probability values are two-sided, and values of $p < 0.05$ were considered statistically significant. Statistical analyses were carried out using OriginPro9 (Origin-Lab) and SPSS (IBM) software packages.

## Supplementary Material

Refer to Web version on PubMed Central for supplementary material.

## Acknowledgments

We thank N. McDannold and N. Vykhodtseva (Focused Ultrasound Lab, Harvard Medical School) for helpful advice on acoustic actuation, C. G. Levins and C. Kastrup for constructive discussions, L. Thapa for assistance with processing animal tissues and J. Mitchell for editing this manuscript. We also thank Koch Institute's Nanotechnology Materials Core Facility for their cryogenic transmission electron microscopy service. This work was funded by the National Institute of Health, Centers for Cancer Nanotechnology Excellence (U54 CA151884). B.C. was a recipient of MIT-Harvard Center for Cancer Nanotechnology Excellence fellowship and the NIH NIBIB Postdoctoral National Research Service Award (1F32EB015835-01).

## References


1. Xu L, Anchordoquy T. Drug Delivery Trends in Clinical Trials and Translational Medicine: Challenges and Opportunities in the Delivery of Nucleic Acid-Based Therapeutics. J Pharm Sci. 2011; 100:38–52. [PubMed: 20575003]
2. Zhang Y, Satterlee A, Huang L. *In Vivo* Gene Delivery by Nonviral Vectors: Overcoming Hurdles? Mol Ther. 2012; 20:1298–1304. [PubMed: 22525514]
3. Kullberg M, McCarthy R, Anchordoquy TJ. Systemic Tumor-Specific Gene Delivery. J Controlled Release. 2013; 172:730–736.
4. Al-Dosari MS, Gao X. Nonviral Gene Delivery: Principle, Limitations, and Recent Progress. AAPS J. 2009; 11:671–681. [PubMed: 19834816]
5. Yang J, Liu HM, Zhang X. Design, Preparation and Application of Nucleic Acid Delivery Carriers. Biotechnol Adv. 2014; 32:804–817. [PubMed: 24239630]
6. Zhu L, Mahato RI. Lipid and Polymeric Carrier-Mediated Nucleic Acid Delivery. Expert Opin Drug Delivery. 2010; 7:1209–1226.
7. Monck MA, Mori A, Lee D, Tam P, Wheeler JJ, Cullis PR, Scherrer P. Stabilized Plasmid-Lipid Particles: Pharmacokinetics and Plasmid Delivery to Distal Tumors Following Intravenous Injection. J Drug Targeting. 2000; 7:439–452.
8. Salem ML, Gillanders WE, Kadima AN, El-Naggar S, Rubinstein MP, Demcheva M, Vournakis JN, Cole DJ. Review: Novel Nonviral Delivery Approaches for Interleukin-12 Protein and Gene Systems: Curbing Toxicity and Enhancing Adjuvant Activity. J Interferon Cytokine Res. 2006; 26:593–608. [PubMed: 16978064]
9. Volkmann X, Fischer U, Bahr MJ, Ott M, Lehner F, Macfarlane M, Cohen GM, Manns MP, Schulze-Osthoff K, Bantel H. Increased Hepatotoxicity of Tumor Necrosis Factor-Related Apoptosis-Inducing Ligand in Diseased Human Liver. Hepatology. 2007; 46508:1498. [PubMed: 17705261]
10. Villemejane J, Mir LM. Physical Methods of Nucleic Acid Transfer: General Concepts and Applications. Br J Pharmacol. 2009; 157:207–219. [PubMed: 19154421]
11. Panje CM, Wang DS, Willmann JK. Ultrasound and Microbubble-Mediated Gene Delivery in Cancer Progress and Perspectives. Invest Radiol. 2013; 48:755–769. [PubMed: 23697924]
12. Lentacker I, Wang N, Vandenbroucke RE, Demeester J, De Smedt SC, Sanders NN. Ultrasound Exposure of Lipoplex Loaded Microbubbles Facilitates Direct Cytoplasmic Entry of the Lipoplexes. Mol Pharmaceutics. 2009; 6:457–467.
13. Burke CW, Suk JS, Kim AJ, Hsiang YHJ, Klibanov AL, Hanes J, Price RJ. Markedly Enhanced Skeletal Muscle Transfection Achieved by the Ultrasound-Targeted Delivery of Non-Viral Gene Nanocarriers with Microbubbles. J Controlled Release. 2012; 162:414–421.
14. Peeters L, Jones A, Demeester J, De Smedt S, Sanders N. Post-PEGylated Lipoplexes are Promising Vehicles for Gene Delivery in RPE Cells. J Controlled Release. 2007:208–217.
15. Ho EA, Osooly M, Strutt D, Masin D, Yang YJ, Yan H, Bally M. Characterization of Long-Circulating Cationic Nanoparticle Formulations Consisting of a Two-Stage PEGylation Step for the Delivery of siRNA in a Breast Cancer Tumor Model. J Pharm Sci. 2013; 102:227–236. [PubMed: 23132529]
16. Khargharia S, Baumhover NJ, Crowley ST, Duskey J, Rice KG. The Uptake Mechanism of PEGylated DNA Polyplexes by the Liver Influences Gene Expression. Gene Ther. 2014; 21:1021–1028. [PubMed: 25253445]
17. Gjetting T, Arildsen NS, Christensen CL, Poulsen TT, Roth JA, Handlos VN, Poulsen HS. *In Vitro* and *In Vivo* Effects of Polyethylene Glycol (PEG)-Modified Lipid in Dotap/Cholesterol-Mediated Gene Transfection. Int J Nanomed. 2010; 5:371–383.
18. Fraga M, Bruxel F, Diel D, de Carvalho TG, Perez CA, Magalhaes-Paniago R, Malachias A, Oliveira MC, Matte U, Teixeira HF. PEGylated Cationic Nanoemulsions Can Efficiently Bind and Transfect pIDUA in a Mucopolysaccharidosis Type I Murine Model. J Controlled Release. 2015; 209:37–46.

19. Mounkes LC, Zhong W, Cipres-Palacin G, Heath TD, Debs RJ. Proteoglycans Mediate Cationic Liposome-DNA Complex-Based Gene Delivery *In Vitro* and *In Vivo*. J Biol Chem. 1998; 273:26164–26170. [PubMed: 9748298]

20. Hattori Y, Yamasaku H, Maitani Y. Anionic Polymer-Coated Lipoplex for Safe Gene Delivery into Tumor by Systemic Injection. J Drug Targeting. 2013; 21:639–647.

21. Allen TM, Sapra P, Moase E. Use of the Post-Insertion Method for the Formation of Ligand-Coupled Liposomes. Cell Mol Biol Lett. 2002; 7:217–219. [PubMed: 12097921]

22. Rabenstein DL. Heparin and Heparan Sulfate: Structure and Function. Nat Prod Rep. 2002; 19:312–31. [PubMed: 12137280]

23. Jeffs LB, Palmer LR, Ambegia EG, Giesbrecht C, Ewanick S, MacLachlan I. A Scalable, Extrusion-Free Method for Efficient Liposomal Encapsulation of Plasmid DNA. Pharm Res. 2005; 22:362–72. [PubMed: 15835741]

24. Tam P, Monck M, Lee D, Ludkovski O, Leng EC, Clow K, Stark H, Scherrer P, Graham RW, Cullis PR. Stabilized Plasmid-Lipid Particles for Systemic Gene Therapy. Gene Ther. 2000; 7:1867–74. [PubMed: 11110420]

25. Dos Santos N, Allen C, Doppen AM, Anantha M, Cox KAK, Gallagher RC, Karlsson G, Edwards K, Kenner G, Samuels L, Webb MS, Bally MB. Influence of Poly(Ethylene Glycol) Grafting Density and Polymer Length on Liposomes: Relating Plasma Circulation Lifetimes to Protein Binding. Biochim Biophys Acta, Biomembr. 2007; 1768:1367–1377.

26. Morille M, Passirani C, Dufort S, Bastiat G, Pitard B, Coll JL, Benoit JP. Tumor Transfection after Systemic Injection of DNA Lipid Nanocapsules. Biomaterials. 2011; 32:2327–2333. [PubMed: 21185595]

27. Chertok B, David AE, Moffat BA, Yang VC. Substantiating *In Vivo* Magnetic Brain Tumor Targeting of Cationic Iron Oxide Nanocarriers *via* Adsorptive Surface Masking. Biomaterials. 2009; 30:6780–6787. [PubMed: 19782394]

28. Carlsson J, Drevin H, Axen R. Protein Thiolation and Reversible Protein-Protein Conjugation. N-Succinimidyl 3-(2-Pyridyldithio)Propionate, a New Heterobifunctional Reagent. Biochem J. 1978; 173:723–737. [PubMed: 708370]

29. Klein MD, Drongowski RA, Linhardt RJ, Langer RS. A Colorimetric Assay for Chemical Heparin in Plasma. Anal Biochem. 1982; 124:59–64. [PubMed: 7125227]

30. Sims GEC, Snape TJ. A Method for the Estimation of Polyethylene-Glycol in Plasma-Protein Fractions. Anal Biochem. 1980; 107:60–63. [PubMed: 7435960]

31. Kim DH, Costello J, Duncan PB, Needham D. Mechanical Properties and Microstructure of Polycrystalline Phospholipid Monolayer Shells: Novel Solid Microparticles. Langmuir. 2003; 19:8455–8466.

32. Carson AR, McTiernan CF, Lavery L, Hodnick A, Grata M, Leng X, Wang J, Chen X, Modzelewski RA, Villanueva FS. Gene Therapy of Carcinoma Using Ultrasound-Targeted Microbubble Destruction. Ultrasound in Medicine & Biology. 2011; 37:393–402. [PubMed: 21256666]

33. Manthorpe M, Cornefert-Jensen F, Hartikka J, Felgner J, Rundell A, Margalith M, Dwarki V. Gene Therapy by Intramuscular Injection of Plasmid DNA: Studies on Firefly Luciferase Gene Expression in Mice. Hum Gene Ther. 1993; 4:419–431. [PubMed: 8399489]

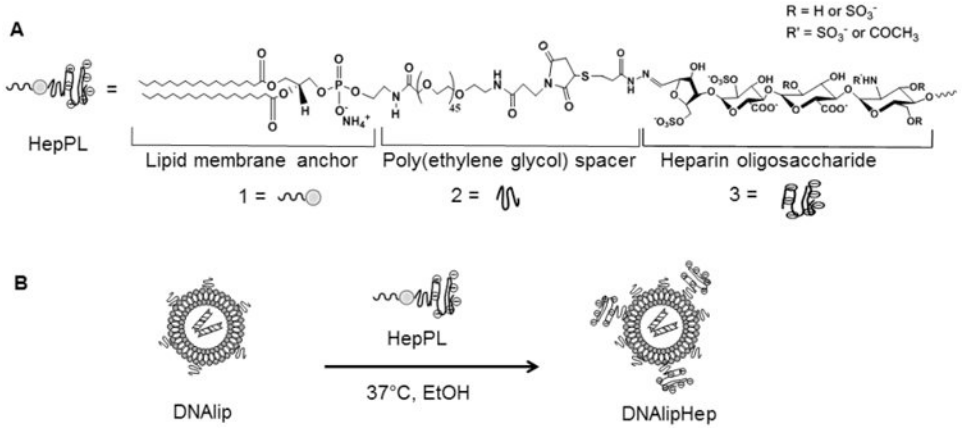


**Figure 1.**

(A) Structure of the lipid–PEG–heparin (HepPL) conjugate comprising (1) lipid membrane anchor, (2) poly(ethylene glycol) 2 kDa spacer, and (3) heparin fragment. (B) Formation of heparin-engrafted DNA liposomes (DNAlipHep) by postinsertion of HepPL conjugate into DNA liposomes (DNAlip).

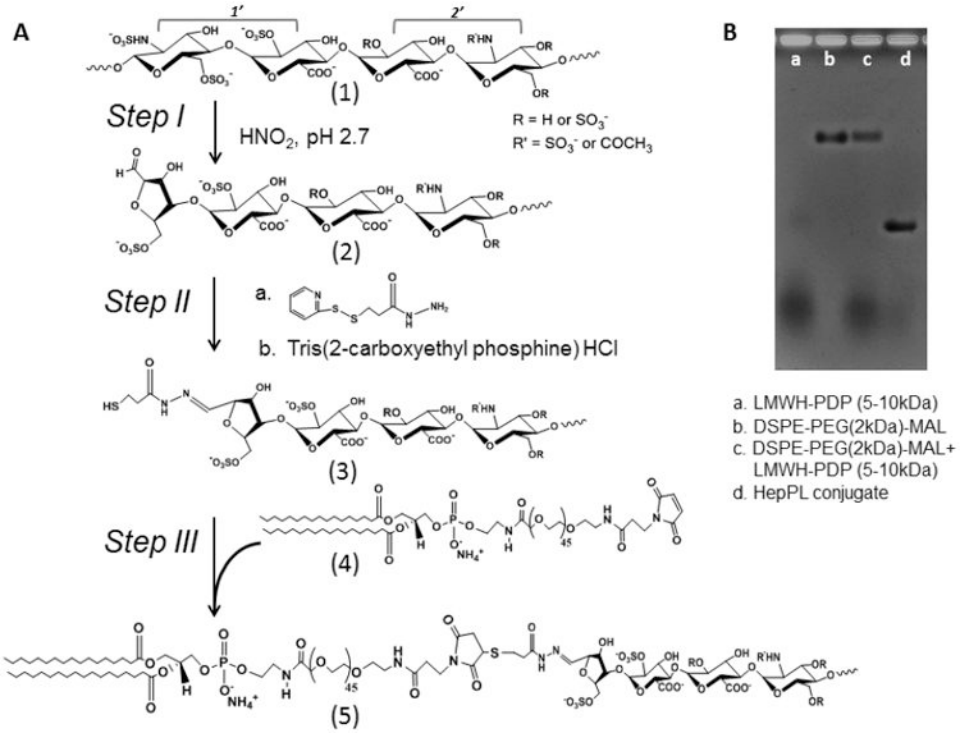


**Figure 2.**

Synthesis of lipid–PEG–heparin (HepPL) conjugate. (A) Three-step reaction scheme for HepPL synthesis; step I, chemical fragmentation of heparin; step II, functionalization of heparin fragments with end-chain sulfhydryl group; step III, conjugation of sulhydryl-modified heparin and maleimide-functionalized lipid–PEG (DSPE-PEG(2 kDa)-MAL) *via* thiol-Michael addition. Compounds: (1) heparin, the structure represents major (1′) and minor (2′) repeating disaccharide subunits of heparin (from ref 22), (2) low molecular weight heparin (LMWH-Ald, 5–10 kDa) fragments with aldehyde-containing terminal 2,5-anhydromannose residue, (3) sulfhydryl-modified LMWH, (4) DSPE-PEG(2 kDa)-MAL, (5) HepPL conjugate. (B) Representative gel electrogram (agarose, 1%) confirming formation of HepPL conjugate; lane a, pyridyldithiopropionate (PDP)-modified LMWH (LMWH-PDP); lane b, DPSE-PEG(2 kDa)-MAL; lane c, physical mixture of DPSE-PEG(2 kDa)-MAL and LMWH-PDP; lane d, HepPL conjugate.

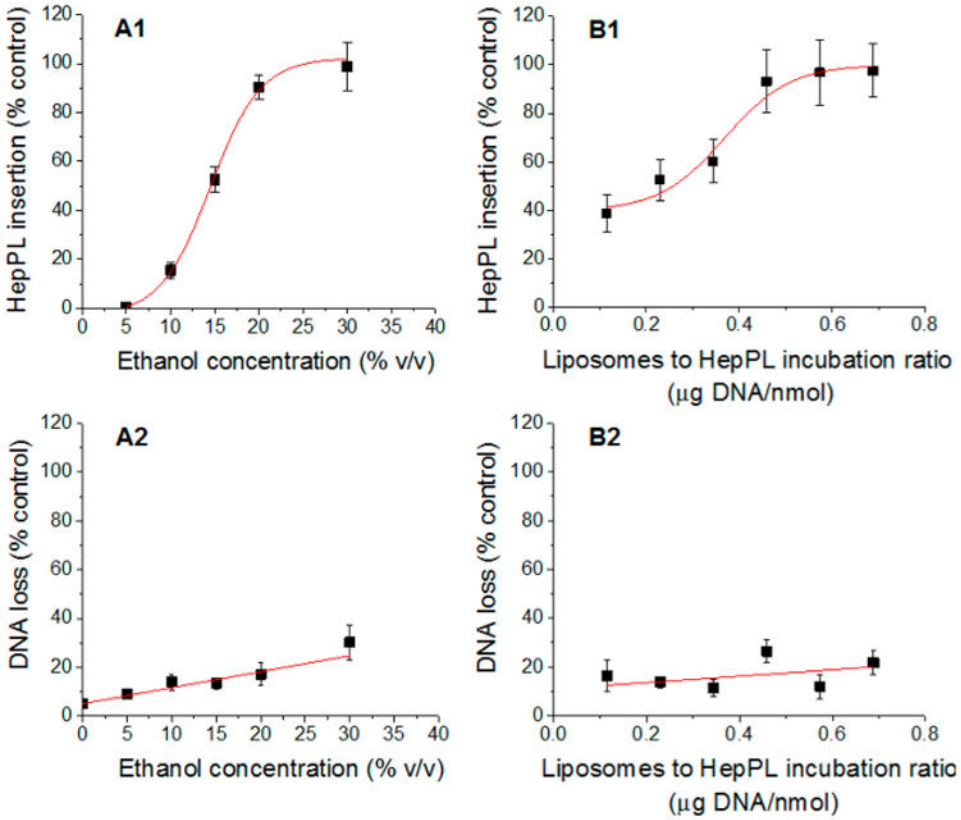


**Figure 3.**

Optimization of postinsertion procedure for incorporation of HepPL into preformed DNA liposomes. (A) Dependence of postinsertion efficiency (A1) and liposomal DNA loss (A2) on ethanol concentration (liposome-to-HepPL incubation ratio = 0.7, $T$ = 37 °C). Postinsertion efficiency data were fitted to a four-parameter nonlinear logistic model; $R^2$ = 0.99, $p$ = 0.03. DNA loss data were fitted to a linear model, $R^2$ = 0.93, $p$ = 0.001. (B) Dependence of postinsertion efficiency (B1) and liposomal DNA loss (B1) on liposome-to-HepPL incubation ratios (ethanol concentration =20%, $T$ = 37 °C); postinsertion efficiency data were fitted to a four-parameter nonlinear logistic model; $R^2$ = 0.92, $p$ = 0.007. DNA loss data were fitted to a linear model, $R^2$ = 0.01; $p$ = 0.36. Data (black) are presented as mean ± S.D., $n$ = 3. Fitted curves (red) are described in Supporting Information.

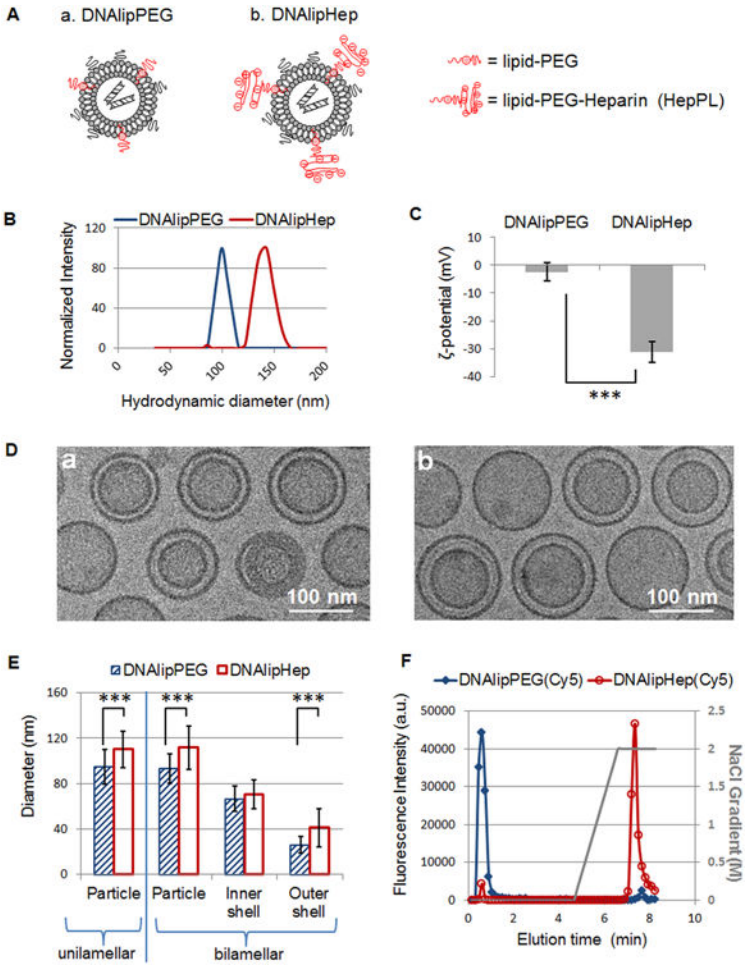


**Figure 4.**

Characterization of heparinized DNA liposomes (DNAlipHep) and PEGylated control DNA liposomes (DNAlipPEG). (A) Schematic depiction of DNAlipPEG and DNAlipHep that contain the lipid–PEG and the lipid–PEG–heparin inserts (red), respectively. (B) Representative dynamic light scattering (DLS) size distribution of DNAlipHep and DNAlipPEG liposomes dispersed in phosphate-buffered saline (PBS), pH 7.4. (C) Zeta-potential of DNAlipHep and DNAlipPEG liposomes dispersed in PBS, pH 7.4. Data represent mean ± S.D, $n = 4$. D. Representative cryoTEM micrographs of DNAlipPEG (a) and DNAlipHep (b) liposomes. (E) Quantitative size analysis of DNAlipPEG and DNAlipHep liposomes (unilamellar and bilamellar subpopulations) based on cryoTEM micrographs; Data represent mean ± S.D., $n = 70$ for each bar. (F) Anion exchange chromatographs for DNAlipHep and DNAlipPEG using columns with a quaternary-ammonium matrix. Statistical comparisons are based on unpaired *t* test. Asterisks denote statistically significant difference: $*p < 0.05$, $**p < 0.01$, $***p < 0.001$.

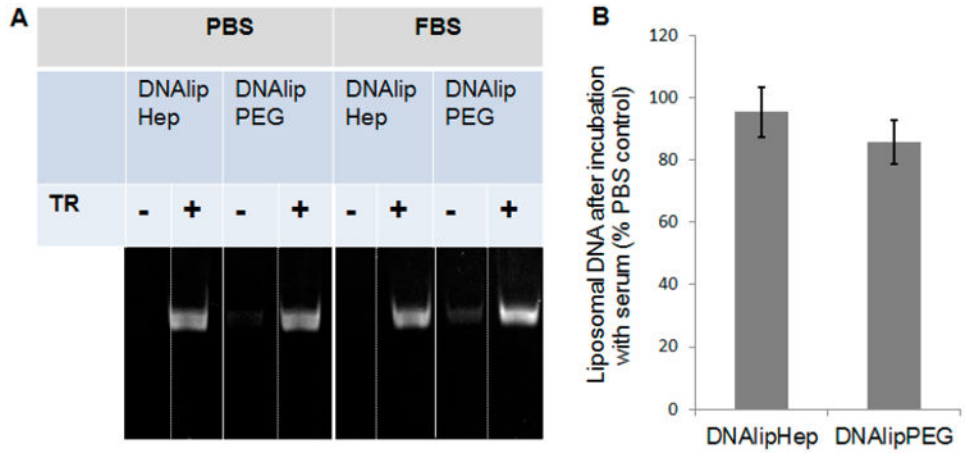


**Figure 5.**

Liposomal stability in the presence of serum. (A) Representative gel electrograms (agarose, 0.8%) of DNAlipHep and DNAlipPEG following incubation of liposomes (50 $\mu$g/mL) with serum (50% fetal bovine serum, FBS) or phosphate-buffered saline (PBS) at 37 °C for 30 min. Each sample was analyzed with and without 0.1% Triton X-100 (Tr) to determine liposome-encapsulated and free DNA, respectively. (B) Quantification of DNAlipHep and DNAlipPEG stability in the presence of serum as compared to PBS controls. Data represent mean ± S.D., $n = 3$. Statistical comparison is based on unpaired $t$ test; $p = 0.26$.

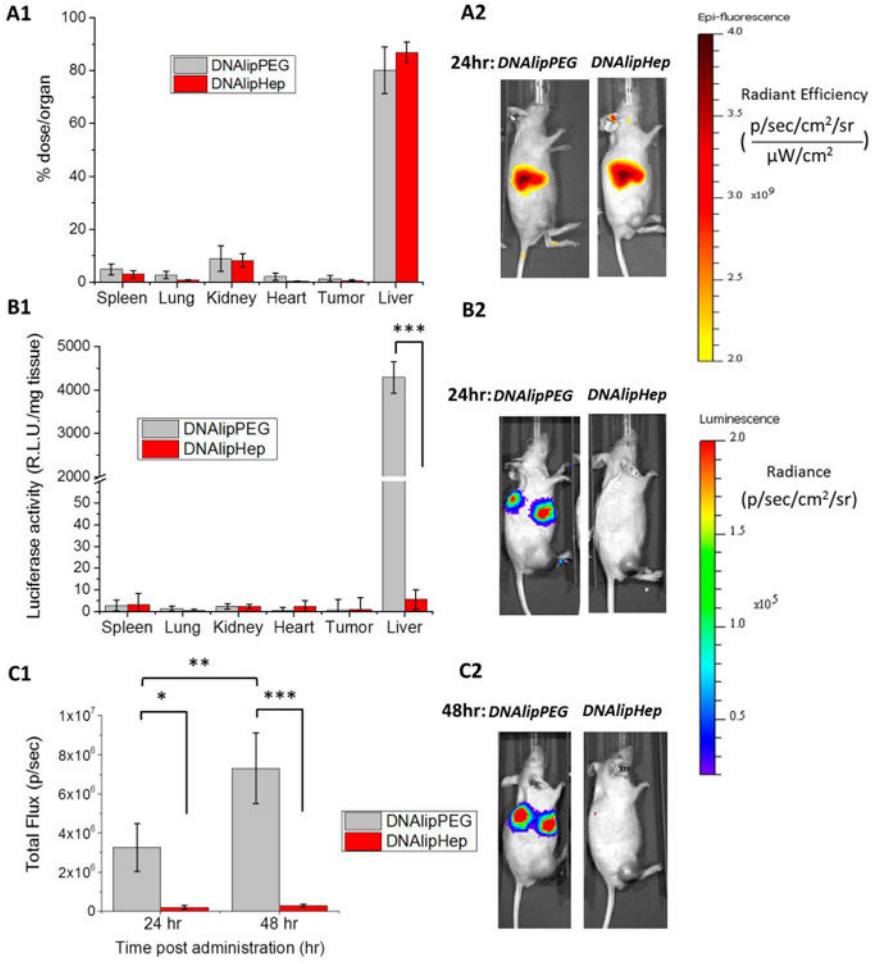


**Figure 6.**

*In vivo* biodistribution and gene expression profiles following intravenous administration of DNAlipHep and DNAlipPEG in tumor-bearing mice. (A1) Organ biodistribution of DNAlipHep and DNAlipPEG quantified *ex vivo* by fluorescence spectrophotometry 24 h post administration. Data represent mean ± S.D., $n = 4$. Statistical comparisons for each organ are based on unpaired *t* test. (A2) Representative qualitative biodistribution profiles analyzed with *in vivo* whole-body fluorescence imaging 24 h post administration. (B1) *In vivo* gene expression profiles following intravenous administration of DNAlipHep and DNAlipPEG, quantified *ex vivo* using luciferase activity assay 24 h post administration. Data represent mean ± S.D., $n = 4$. Statistical comparisons for each organ are based on unpaired *t* test. (B2) and (C2) Representative qualitative profiles of luciferase gene expression analyzed with *in vivo* whole-body bioluminescence imaging 24 h (B2) and 48 h (C2) postadministration. (C1) Total luminescence flux (measured in photons per second (p/sec)) for the liver ROI at 24 and 48 h postadministration of DNAlipHep and DNAlipPEG. Data represent mean ± S.D., $n = 3$. Statistical comparisons were made using the one-way ANOVA, followed by *post hoc* Tukey's pairwise tests. Asterisks denote statistical significance,* $p < 0.05$, ** $p < 0.01$, *** $p < 0.001$; R.L.U., relative light units; ANOVA, analysis of variance; SD, standard deviation.

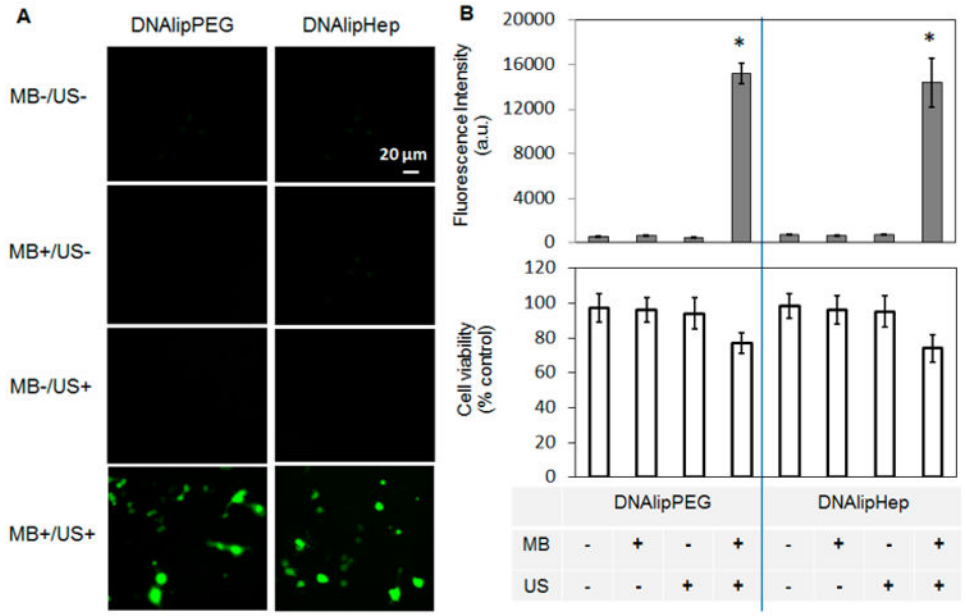


**Figure 7.**

*In vitro* UTMD-mediated GFP gene transfer with DNAlipHep and DNAlipPEG liposomes carrying GFP-encoding plasmid DNA in HeLa cells. UTMD treatment is compared to controls with and without microbubbles (MB) and ultrasound (US). (A) Representative fluorescence micrographs of HeLa cells following exposure to (1) liposomes only without microbubbles or ultrasound (MB−/US−), (2) liposomes and microbubbles without ultrasound (MB+/US−), (3) liposomes and ultrasound without microbubbles (MB−/US+), and (4) liposomes with microbubbles and ultrasound (the UTMD protocol; MB+/US+). Left and right panels depict micrographs for DNAlipPEG and DNAlipHep liposomes, respectively. (B) Quantitative analysis of GFP transfection (top), and cell viability (bottom) using fluorescence spectroscopy and Trypan Blue assay, respectively, under conditions described in (A). Data represent mean ± S.D., $n = 4$. Statistical analysis is based on one-way ANOVA, followed by *post hoc* Tukey's pairwise comparisons. Asterisks denote statistically significant difference *versus* MB−/US− group, *$p < 0.05$, **$p < 0.01$, ***$p < 0.001$. ANOVA, analysis of variance; SD, standard deviation.

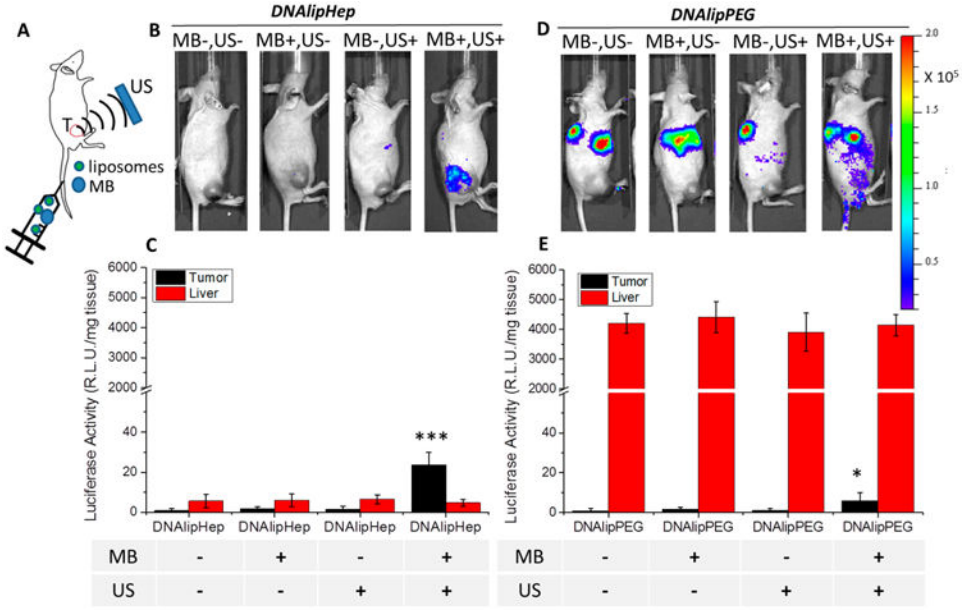


**Figure 8.**

Effect of tumor-directed UTMD on gene expression profiles following intravenous administration of DNAlipHep and DNAlipPEG liposomes. (A) Schematic depiction of tumor-directed ultrasound-targeted microbubble destruction (UTMD); microbubble-collapsing ultrasound (US) beam is applied to the tumor (T) following intravenous coadministration of liposomes and microbubbles (MB). (B) and (D) Representative qualitative profiles of luciferase gene expression following i.v. administration of DNAlipHep (B) or DNAlipPEG (D) with and without microbubbles/ultrasound. Gene expression was analyzed using *in vivo* whole-body bioluminescence imaging. Color bar represents radiance expressed as photon flux per second per square centimeter per steradian (p/sec/cm$^2$/sr). (C) and (E) *Ex vivo* quantification of tumor and liver gene expression following i.v. administration of DNAlipHep (C) and DNAlipPEG (E) with and without microbubbles/ultrasound. Gene expression was analyzed using luciferase activity assay. Data represent mean ± S.D., $n = 4$. Statistical comparison of gene expression under different experimental conditions (MB−/US−, MB+/US−, MB−/US+, MB+/US+) were made for each organ (liver or tumor) using the one-way ANOVA, followed by *post hoc* Tukey's pairwise tests. Asterisks denote statistical significance *versus* MB−/US− group, *$p < 0.05$, **$p < 0.01$, ***$p < 0.001$. R.L.U., relative light units; ANOVA, analysis of variance; SD, standard deviation.

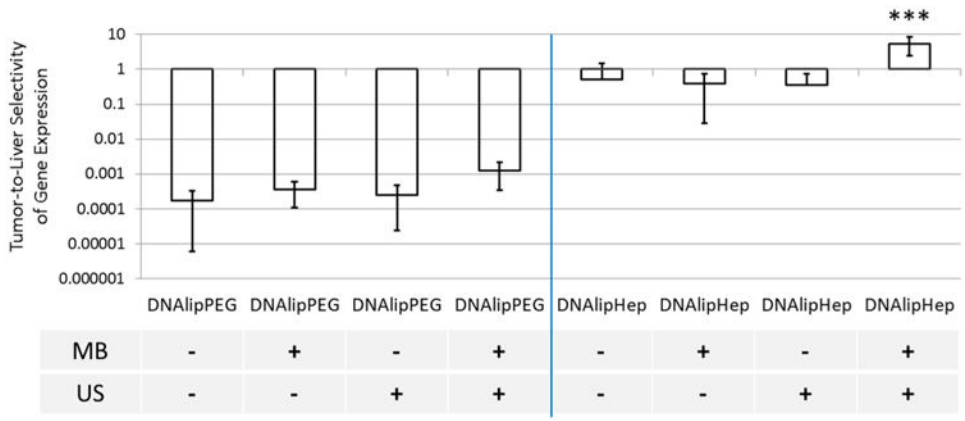


**Figure 9.**

Tumor-to-liver selectivity of gene expression for DNAlipHep and DNAlipPEG liposomes with and without UTMD. Data represent mean ± S.D., $n = 4$. Statistical comparisons were made using the one-way ANOVA, followed by *post hoc* Tukey's pairwise tests; Asterisks denote statistical significance, $*p < 0.05$, $**p < 0.01$, $***p < 0.001$. ANOVA, analysis of variance; SD, standard deviation.